

Review

Molecular Engineering of Redox Couples for Non-Aqueous Redox Flow Batteries

Casey M. Davis ¹, Claire E. Boronski ¹, Tianyi Yang ², Tuo Liu ³ and Zhiming Liang ^{4,*}¹ Department of Chemistry, University of Colorado, Boulder, CO 80309, USA² Research and Development, Corden Pharma Colorado, Boulder, CO 80301, USA³ Department of Chemistry, University of Kentucky, Lexington, KY 40506, USA⁴ Department of Mechanical Engineering, University of Colorado, Boulder, CO 80309, USA

* Correspondence: zhli7266@colorado.edu

Abstract: Redox flow batteries (RFBs) have attracted significant attention as a promising electrochemical energy storage technology, offering various advantages such as grid-scale electricity production with variable intermittent electricity delivery, enhanced safety compared to metal-ion batteries, decoupled energy and power density, and simplified manufacturing processes. For this review, we exclusively focus on organic, non-aqueous redox flow batteries. Specifically, we address the most recent progress and the major challenges related to the design and synthesis of robust redox-active organic compounds. An extensive examination of the synthesis and characterization of a wide spectrum of redox-active molecules, focusing particularly on derivatives of posolytes such as quinone, nitroxyl radicals, dialkoxybenzenes, and phenothiazine and negolytes such as viologen and pyridiniums, is provided. We explore the incorporation of various functional groups as documented in the references, aiming to enhance the chemical and electrochemical stability, as well as the solubility, of both the neutral and radical states of redox-active molecules. Additionally, we offer a comprehensive assessment of the cell-cycling performance exhibited by these redox-active molecules.

Keywords: redox flow batteries; non-aqueous; organic; molecular engineering

Citation: Davis, C.M.; Boronski, C.E.; Yang, T.; Liu, T.; Liang, Z. Molecular Engineering of Redox Couples for Non-Aqueous Redox Flow Batteries. *Batteries* **2023**, *9*, 504. <https://doi.org/10.3390/batteries9100504>

Academic Editor: Dino Tonti

Received: 1 September 2023

Revised: 29 September 2023

Accepted: 2 October 2023

Published: 4 October 2023



Copyright: © 2023 by the authors. Licensee MDPI, Basel, Switzerland. This article is an open access article distributed under the terms and conditions of the Creative Commons Attribution (CC BY) license (<https://creativecommons.org/licenses/by/4.0/>).

1. Introduction

Redox flow batteries (RFBs) represent a highly promising electrochemical energy storage technology that offers several advantages, including (i) the controllable delivery of variable intermittent electricity for grid-scale power production; (ii) improved safety compared to metal-ion batteries; (iii) decoupled energy and power density; and (iv) simplified manufacturing processes [1–5]. A standard RFB configuration contains reservoirs that store redox-active electrolytes, electrodes, membranes, and flow circulation systems (Figure 1). The redox species produced by the positive and negative active materials (posolyte and negolyte) serve to store and release energy. As illustrated in Figure 1, in the charging process, the posolyte undergoes oxidation, releasing electrons, while the negolyte undergoes reduction, accepting the electrons. This redox reaction facilitates energy storage in the form of potential [6]. Conversely, during discharging, the reverse reaction takes place, releasing the stored energy as electrical energy. In RFB systems, the energy density can be quantified using the equation $U = \frac{nCFV}{\mu_v}$, where U represents energy density, n is the number of electrons in the redox reaction, C denotes the concentration of electrolytes, F stands for Faraday's constant, V is the voltage of the battery, and μ_v is the volume factor, which is calculated as $\mu_v = 1 + (\text{lower electrolyte concentration}/\text{higher electrolyte concentration})$ [7,8]. Consequently, increasing the concentration and redox potential of redox-active species will increase the energy density of the RFBs.

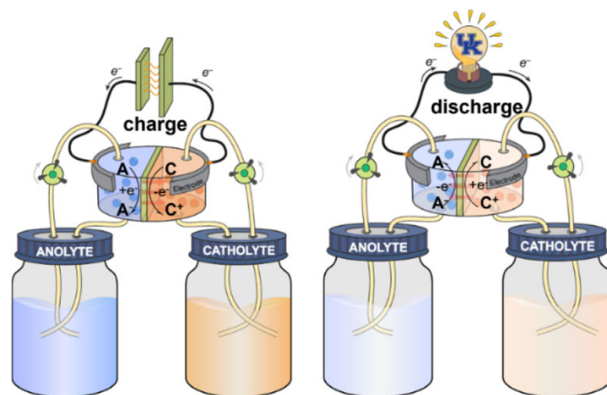


Figure 1. Schematic of a redox flow battery (A = anolyte; C = catholyte). In the charge process, the posolyte (catholyte) releases electrons and undergoes oxidation, while the negolyte (anolyte) gains electrons and experiences reduction. This redox reaction is reversed during the discharge process [9].

Traditional aqueous redox flow batteries (ARFBs) employ water as a solvent to enable electrochemical reactions. The most promising of the aqueous RFBs thus far are vanadium redox flow batteries [10,11]. Nevertheless, the constrained operating voltage range (<1.3 V) [9,12] and high freezing temperature of water ($\geq 0^\circ\text{C}$) impose limitations on achieving higher energy density and broader geographic applicability for RFBs [9]. Particularly, in regions with average winter temperatures ranging between -10 and -40°C at northern latitudes above 30° , these constraints become even more pronounced [13]. Unlike ARFB, non-aqueous redox flow batteries (NAORFBs) have wider operating voltages and temperature ranges, achieved by employing organic solvents in lieu of water. Table 1 summarizes the physical and chemical properties of the most used organic solvents in NAORFBs [14]. Typically, the freezing point of organic solvents is below -40°C , providing a wider electrochemical window (>5 V) [15]. This creates more favorable conditions for operating high-energy-density redox flow cells.

Table 1. Physical and chemical characteristics of organic solvents used in NAORFBs [16,17].

	Freezing Point ($^\circ\text{C}$)	Boiling Point ($^\circ\text{C}$)	Viscosity (mPa s^{-1})	Size of Electrochemical Windows (V)
Acetonitrile (ACN)	-44	82	0.34	6.1
Propylene carbonate (PC)	-49	242	2.53	6.6
N-methyl-2-pyrrolidone (NMP)	-24	204	1.7	5.4
Dichloromethane (DCM)	-95	40	0.39	4.9
Tetrahydronfuran (THF)	-108	66	0.46	5.5

Redox-active organic molecules are of particular interest for low-cost RFBs because they are synthesized from the earth's abundant elements (e.g., carbon, hydrogen, oxygen, etc.) [18–20]. Furthermore, the organic functional groups provide opportunities to modify physical and electrochemical properties such as solubility, chemical and electrochemical stability, redox potential, ionic conductivity, and reaction kinetics to better meet high-performance requirements [5,21–24]. Over the last few decades, molecular frameworks like posolytes, including anthraquinone [25–28], nitroxyl radicals [29–32], dialkoxybenzenes [33–35], and phenothiazine [9,21,23,36–38], as well as negolytes like viologen [39–42] have garnered significant attention as potential redox-active materials for energy storage applications. While their unique properties hold great promise, challenges including (1) low solubility; (2) poor electrochemical stability of radicals; (3) low redox potential; and (4) low ionic conductivity still prevent these materials from being used in commercial applications [3,43]. To address these limitations, recent efforts in molecular

engineering have focused on the design and synthesis of derivatives based on these core structures [44]. These modifications aim to enhance the solubility and the chemical and electrochemical stability of redox-active species, paving the way for the development of high-energy-density redox flow batteries. By tailoring the molecular structures of these redox-active materials, researchers strive to achieve significant improvements in their performance, thereby overcoming the barriers that have hindered their practical application in energy storage systems. These advancements hold the potential to unlock the full capabilities of these molecular cores, making them viable candidates for next-generation RFBs and other cutting-edge energy storage technologies.

This review primarily focuses on organic active materials within organic solvents. These organic, non-aqueous flow batteries present a unique set of potentials and challenges different from those of inorganic and aqueous flow batteries. In particular, we have provided a comprehensive summary and analysis of the synthesis and characterization of a diverse range of redox-active organic molecules, with a particular focus on derivatives of quinones, nitroxyl radicals, dialkoxybenzenes, phenazines, pyridiniums, viologens, and phenothiazines. We have elucidated the utilization of various functional groups, such as methyl groups and glycol chains, to enhance chemical and electrochemical stability, the solubility of neutral and radical salts, and the overall potential performance of these redox-active species. Moreover, in-depth evaluations of the full cell-cycling performances of these redox-active posolytes and negolytes are also discussed. By collating and presenting a comprehensive overview of the synthesis, characterization, and performance of these redox-active molecules, we aim to contribute to the advancement of redox-active materials and inspire further innovations in redox flow battery systems.

2. Cathodic Redox-Active Organic Molecules

While other components, such as membranes, can impact electrochemistry, it is important to note that the chemistries of the catholyte and anolyte are the primary drivers of cycling performance in RFBs [45,46]. A more negative or positive redox potential enables a higher-voltage battery coupled with increased solubility, thereby enhancing the battery's energy density [47,48]. Both chemical and electrochemical stability are crucial for ensuring the long-term durability of RFBs. Therefore, it is crucial to optimize electrolytes in terms of redox potential, solubility, and both chemical and electrochemical stability. Low energy density is often pointed to as an inhibitor of NAORFBs due to the low solubility of redox-active molecules, making it a critical aspect to improve [49,50]. For this reason, efforts in areas such as molecular engineering have been taken to customize the solubility of redox-active compounds [24,51,52]. Among the redox-active core structures of catholytes, quinones, nitroxyl radicals, phenothiazine, and dialkoxybenzenes have demonstrated remarkable success owing to their stable structures. These molecules, upon oxidation, form radicals or charge species that are stabilized by conjugated rings, resulting in enhanced stability of the charged molecules. Here, we describe promising catholyte categories and how derivatives have been developed to further the aforementioned metrics.

2.1. Quinones and Derivatives

The stability of quinone radicals can be attributed to their unique molecular structures and electronic configurations [53–55]. As Figure 2a shows, quinone radicals possess a conjugated π -electron system, creating a resonance stabilization effect. This delocalization of electrons helps distribute charge density, resulting in a more stable radical species. Figure 2b summarizes a series of reported quinone derivatives for which electron-withdrawing or -donating functional groups are present on the quinone ring to adjust either solubility or redox potential. Their redox potential can vary within the range of 2.2 to 4 V, while their solubility in dimethylacetamide (DMA) can vary by up to 1 M (Table 2).

Quinone derivatives have been studied extensively for battery applications, often as lithium-ion battery cathode materials [56–58]. Anthraquinone (AQ) was originally reported for use in aqueous redox flow batteries by Aziz's group in 2014, with much of the research

thereafter continuing to focus on aqueous chemistries [25,59,60]. For both aqueous and non-aqueous RFBs, anthraquinones are touted as the most promising molecules of the natural organic materials, partially due to their relatively high electrochemical stability and straightforward, cost-effective synthesis [61]. The redox potential of quinone derivatives tends to be between 2 and 3 V vs. Li⁺/Li, and the variations in this redox potential can be attributed to the aromaticity of the molecular backbone and the influence of the substituents [62]. For example, 1,4-benzoquinone (BQ) has a redox potential of 2.8 vs. Li⁺/Li, while anthraquinone (AQ) has a redox potential of 2.25 V vs. Li⁺/Li (Table 2).

Most quinone-based compounds have low solubilities (<0.05 M) in polar organic solvents. To improve their solubility, the modification of the quinone core is often necessary [26]. Wang et al. studied a modified anthraquinone, 1,5-bis(2-(2-methoxyethoxy)ethoxy)anthracene-9,10-dione (15D3GAQ), to which two triethylene glycol monomethyl ether groups have been added as compared to classic anthraquinone molecules (Figure 2c). These additions increase solubility, and, although the solubilities of this compound were not reported by the group, they were able to cycle 0.25 M of 15D2GAQ in a 1.0 M LiPF₆/PC solution as a catholyte against lithium metal (Figure 3a). The capacity faded over time, which was ascribed to side reactions between carbonate solvents and the anthraquinones. This fading of capacity has been noted before for similar quinone compounds [26,63]. Pahlevaninezhad et al. developed a high-electrode-potential (4 V vs. Li⁺/Li), four-electron-transfer quinone, tetra-aminoanthraquinone (DB-1), with a 111 mAh discharge capacity and near-100% capacity retention over 50 cycles at a 1 M concentration in dimethyl sulfoxide. This demonstrates the use of derivatives to improve capacity retention and solubility (Figure 3b) [64]. Zheng et al. cycled a fairly standard derivative of quinone, methyl-p-benzoquinone (MBQ). MBQ appeared to be less stable and have a weaker oxidizing potential than many of the other derivatives discussed here (Figure 3c,d) [65]. This instability was believed to be due to the reduction of MBQ to a variety of forms in equilibrium, so, during cycling, MBQ is reduced to states from which it cannot be re-oxidized.

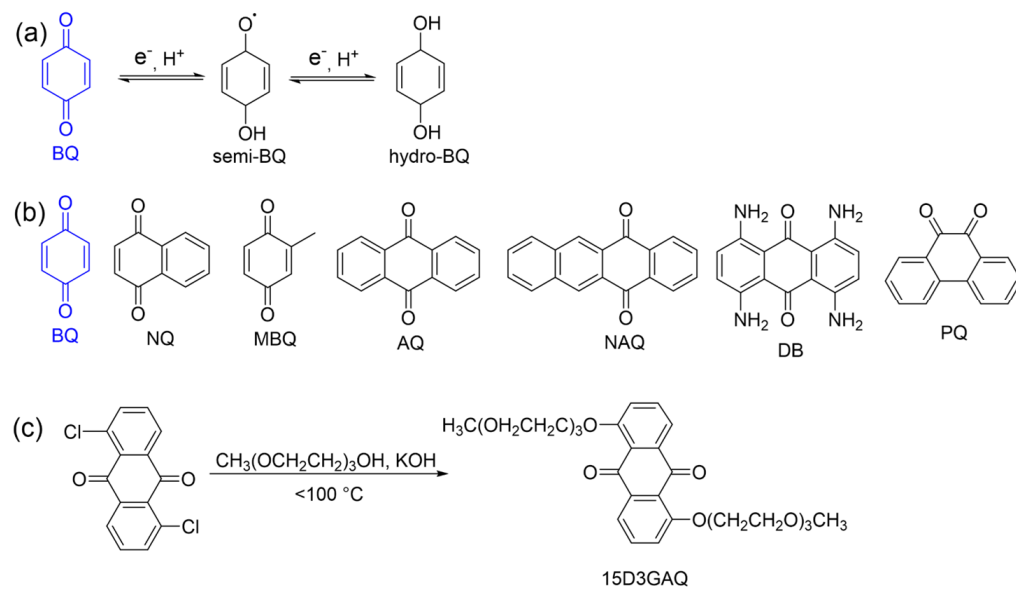


Figure 2. Chemical structures and synthesis of quinone derivatives. (a) Redox reaction of 1,4-benzoquinone (BQ). (b) Chemical structures of anthraquinone derivatives BQ, NQ, MBQ, NAQ, DB, and PQ. (c) Synthesis of 15D3GAQ [26,59,61–63].

Table 2. Electrochemical and physical characteristics of quinone derivatives [26,59,61–63].

Compound	Redox Potential (vs. Li ⁺ /Li)	Diffusion Coefficient ($\times 10^{-6}$ cm ² s ⁻¹)	Solubility (M) Neutral in DMA
AQ	2.25	4.20	<0.1
NAQ	2.2	4.29	<0.1
NQ	2.6	4.63	>0.1
BQ	2.8	5.00	>0.1
PQ	2.7	4.96	0.3
15D3GAQ	2.5	-	>0.25
DB-1	4	-	1
MBQ	-	0.034	-

“-” indicates that no data were provided by the references; DMA is an acronym for dimethylacetamide.

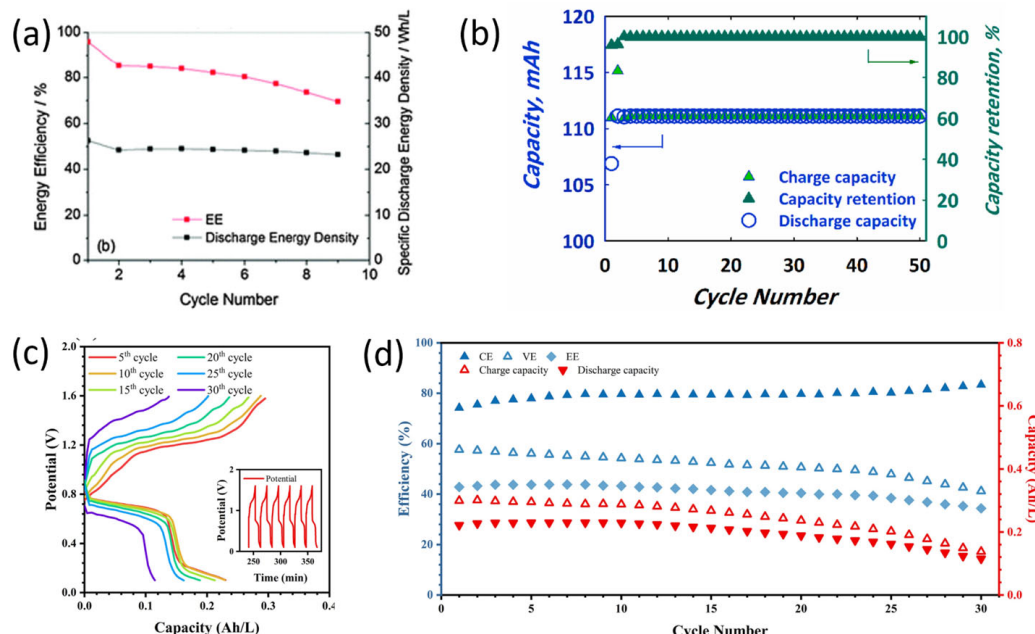


Figure 3. The electrochemical performance of quinone derivatives with lithium metal as the negative electrode. (a) 0.25 M 15D3GAQ in 1.0 M LiPF₆/PC [26] (Reprinted with permission, 2012, Royal Society of Chemistry.) (b) Charge–discharge voltage and current as a function of time with 80 mM of DB-1 (14–15 mL) [64]. (Reprinted with permission, 2012, Royal Society of Chemistry.) (c) Voltage curves of MBQ-TEMPO RFB during galvanostatic cycling at 4 mA cm⁻² [65]. (Reprinted with permission, 2023, Elsevier.) (d) Efficiency, charging capacity, and discharging capacity of MBQ-TEMPO during galvanostatic cycling [65]. (Reprinted with permission, 2023, Elsevier).

2.2. Phenothiazines and Derivatives

The study of phenothiazines for use in non-aqueous organic redox flow batteries has been extensively conducted by Odom’s group [9,21–23,36–38,66–68]. They developed a general synthesis protocol for both neutral (Figure 4) and radical phenothiazine derivatives using anhydrous dichloromethane (DCM), which is mixed with NOBF₄ and then diethyl ether, to form a precipitate. After filtration, the precipitate is dissolved in DCM and then re-precipitated with diethyl ether. The product is then dried under a vacuum [38]. This relatively simple procedure could be repeated for desired phenothiazine derivatives. Initially synthesized and employed as an overcharge protection compound in lithium-ion batteries, N-ethylphenothiazine (EPT) exhibits robust electrochemical stability and holds promise as a potential catholyte for redox flow batteries. Nonetheless, the solubility of neutral EPT remains limited to 0.1 M in organic solvents, posing a challenge when considering its use as a catholyte [38]. N-(2-methoxyethyl)phenothiazine (MEPT) and N-[2-(2-methoxyethoxy)ethyl]phenothiazine (MEEPT) (Figure 4), which have been

modified with glycol chains, exhibit significantly improved solubility compared to EPT (Table 3). MEEPT demonstrates stable galvanostatic cycling as the catholyte in symmetric cells (Figure 5a) and when paired with viologen anolyte (Figure 5b) over hundreds of cycles with minimal capacity decay [36,38]. Both nuclear magnetic resonance (NMR) and cyclic voltammetry (CV) analyses confirmed the absence of decomposition in the MEEPT electrolyte following cycling. While MEEPT exhibits promising cycling performance, it is important to note its instability in the second redox potential. To enhance the stability of the second redox potential without compromising solubility, N-ethyl-3,7-bis(2-(2-methoxyethoxy)ethoxy)phenothiazine (B(MEEO)EPT) was synthesized via introducing oligoglycol chains (Figure 4) [21]. B(MEEO)EPT exhibits stable galvanostatic cycling with a redox potential of 0.65 V vs. $\text{Cp}^2 \text{Fe}^{0+/+}$. During cycling, a 27% capacity fade was observed over 140 cycles, attributed to active species crossover instead of material degradation (Figure 5d).

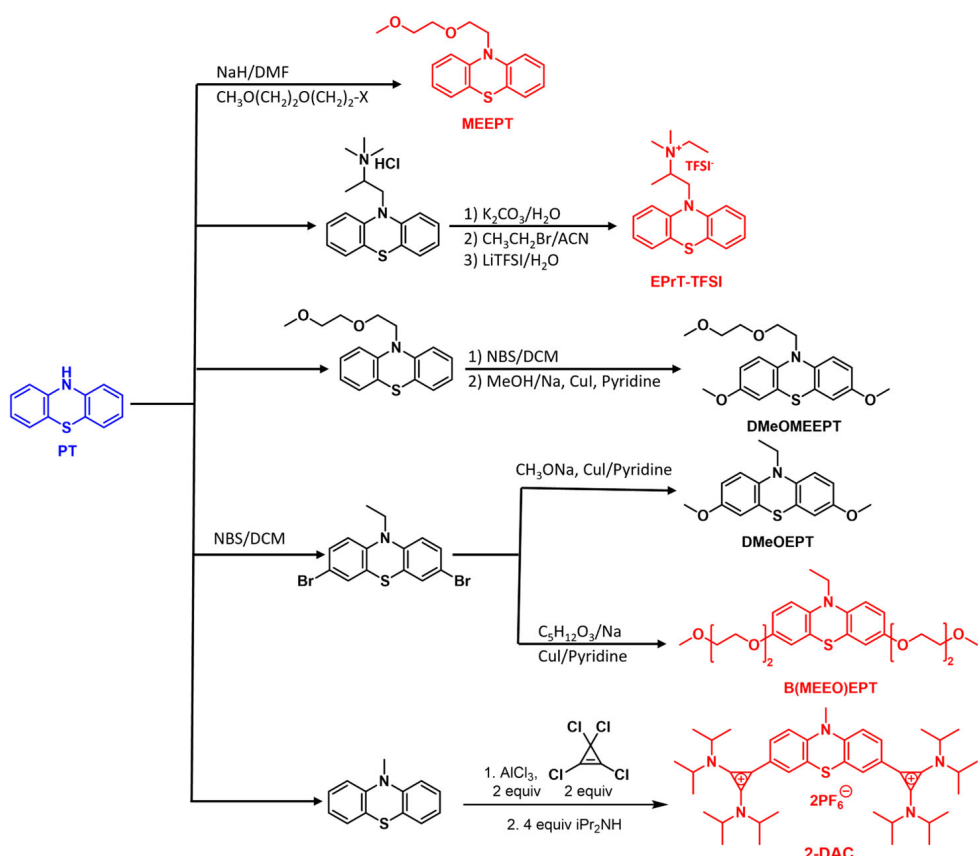


Figure 4. Chemical structures and synthesis of phenothiazine derivatives [21,23,37,38].

Table 3. Physical and chemical properties of phenothiazine derivatives [9,21,23,36–38].

Compound	1st Redox Potential (vs. $\text{Cp}^2 \text{Fe}^{0+/+}$)	2nd Redox Potential (vs. $\text{Cp}^2 \text{Fe}^{0+/+}$)	Diffusion Coefficient ($\times 10^{-6} \text{ cm}^2 \text{s}^{-1}$)	Solubility (M) Neutral	Solubility (M) Radical Salt
EPT	0.278	0.956	2.3	0.11	0.28
MEEPT	0.311	0.937	1.6	miscible	0.55
DMeOEPT	0.056	0.655	1.8	0.06	0.06
DMeOMEEPT	0.093	0.666	1.6	miscible	0.18
B(MEEO)EPT	0.064	0.654	0.8	miscible	0.63
EPRT-TFSI	0.55	1.12	15.3	1.27	1.27
2-DAC	0.6	1.2	5.4	-	0.09
4-DMPP	0.64	1	5.77	miscible	0.45

"—" indicates that no data were provided by the references.

Substituted cyclopropeniums have been heavily studied as catholytes for NARFBs, largely by the Sanford group [69–73]. They noted the straightforward synthesis procedure while also addressing the issues regarding the compound's stability, which they hypothesized might be attributed to the presence of the substituted methyl groups. In response, they replaced the methyl groups with isopropyl substituents, leading to improved stability. However, they encountered challenges related to low solubility and redox potential and high crossover rates, prompting the research group to further explore and evaluate various derivatives. A methyl group was added to the nitrogen atom to enhance the oxidizing reduction potential [70]. In addition to the physical organic analysis of various derivatives, they developed a 1,2-bis(diisopropylamino)-3-cycloprpenylium-functionalized benzene (2-DAC) for a high-potential catholyte (Figure 4). The group significantly increased the redox potential to 1.2 V (vs $\text{Cp}^2 \text{Fc}^{0/+}$) by swapping out substituents on the benzene ring [71]. The electrochemical cycling of 2-DAC exhibited only 3% capacity loss over 50 cycles (Figure 5e), showing the effectiveness of DAC substituents in terms of stability.

While 2-DAC presents a notably stable redox potential in its salt-free electrolyte form, its limited solubility of 0.1 M in MeCN significantly impacts its viability for use in RFBs. A promising alternative, ethylpromethazine bis(trifluoromethanesulfonyl)imide (EPRT-TFSI), introduced by Odom's group, displays a high redox potential of 1.2 V (vs $\text{Cp}^2 \text{Fc}^{0/+}$) along with substantial radical salt solubility of 1.3 M in MeCN and robust electrochemical stability compared to other reported salt-free posolytes [71]. This compound is relatively straightforward to synthesize, involving three steps starting from commercially available promethazine hydrochloride (Figure 4). The process includes deprotonation with aqueous potassium carbonate, the substitution of an ethyl group at the trialkylated N position, and finally anion exchange with a TFSI anion. During cycling of EPRT-TFSI against MEEV-(TFSI)₂, a 43% capacity fade over 73 cycles was observed, which was confirmed via CV and NMR to be due to active species crossover (Figure 5c) [71]. Another derivative of 2-DAC, 2,6-deimethylpiperidine (4-DMPP), was identified as a promising catholyte due to its redox potential, stability, and high solubility (Table 3). When cycled at 0.3 M, it had a capacity retention of 92.5% over 300 cycles (Figure 5f).

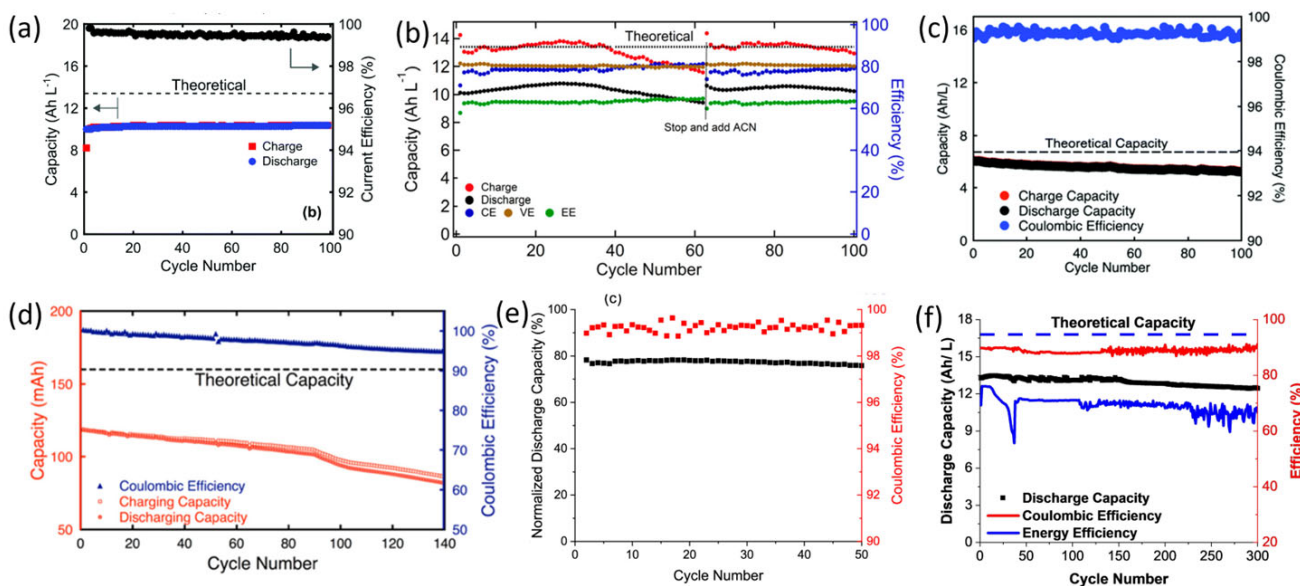


Figure 5. The electrochemical performance of phenothiazine derivatives. (a) Charge and discharge capacities and coulombic efficiency of MEEPT in a symmetric flow cell at 100 mA cm⁻² [38]. (Reprinted with permission, 2016, Royal Society of Chemistry.) (b) Charge and discharge capacities and coulombic efficiency of 0.5 M MEEPT/MEEV-TFSI₂ premixed redox flow cell cycled at 20 mA cm⁻² [36]. (Reprinted with permission, 2021, American Chemical Society.) (c) Charge and discharge capacities and coulombic efficiency of salt-free 0.25 M EPRT-TFSI and MEEV-(TFSI)₂ flow cell cycled at 100 mA cm⁻² [71]. (d) Capacity and coulombic efficiency of 4-DMPP at 0.3 M. (e) Normalized discharge capacity and coulombic efficiency of 4-DMPP at 0.3 M. (f) Discharge capacity, coulombic efficiency, and energy efficiency of 4-DMPP at 0.3 M.

cell at 10 mA cm^{-2} [23]. (Reprinted with permission, 2021, Royal Society of Chemistry.) (d) Constant current cycling of B(MEEO)EPT in a symmetric flow cell at 25 mA cm^{-2} [21]. (Reprinted with permission, 2019, American Chemical Society.) (e) Discharge capacity and coulombic efficiency versus cycle number for cycling of 2.5 mM 1-DAC in 0.5 M TBAPF₆/ACN in a static H-cell [69]. (Reprinted with permission, 2021, American Chemical Society.) (f) Discharge capacities and coulombic efficiency of 0.3 M 4-DMPP and 0.6 M Viologen-5 at 60 mA cm^{-2} [74]. (Reprinted with permission, 2021, John Wiley & Sons).

2.3. TEMPO and Derivatives

(2,2,6,6-Tetramethylpiperidin-1-yl)oxyl (TEMPO) is one of the most studied neutral radicals for energy storage due to its excellent electrochemical stability and solubility [4,32,75–78]. The stability of the TEMPO radical can be attributed to the delocalization resulting from conjugation over the N-O bond, combined with the steric protection provided by its methyl substituents, which effectively prevents dimerization (Figure 6a) [79,80]. Its use in non-aqueous flow batteries is still limited thus far, and the most promising work is discussed here. Li et al. in 2011 reported the use of TEMPO as a catholyte in a non-aqueous redox flow battery, inducing high efficiencies and stability, thereby inspiring interest in TEMPO and TEMPO derivatives [31]. They did not specifically report on capacity, but the coulombic efficiency was relatively high, reaching 90% after 20 cycles. Wang’s group continued this work to demonstrate a high-performance TEMPO organic redox flow battery [32]. TEMPO was found to have a high solubility, redox potential, and diffusion coefficient. After 100 cycles, they found an average capacity retention of 99.8% per cycle, demonstrating the promise of TEMPO (Figure 7a).

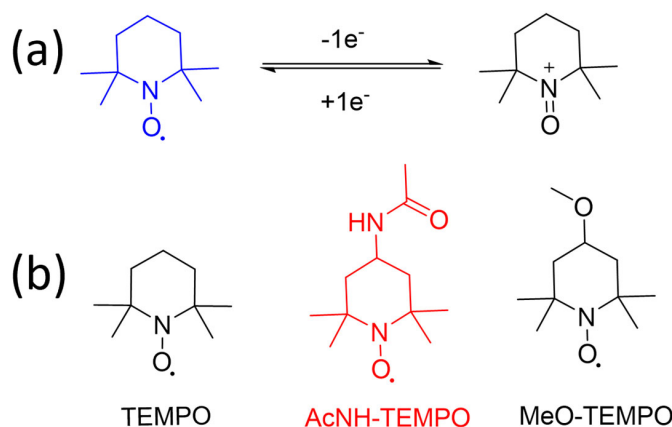


Figure 6. Chemical structures of TEMPO derivatives. (a) The redox process of TEMPO, and (b) Chemical structure of TEMPO, AcNH-TEMPO, and MeO-TEMPO [29,30,32].

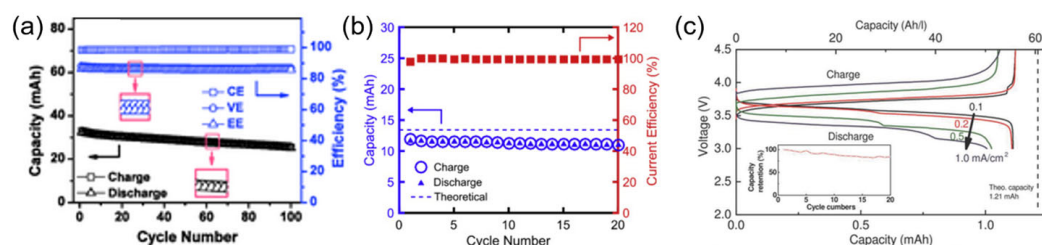


Figure 7. Electrochemical cycling of TEMPO derivatives with (a) 0.1 M TEMPO in 1 M LiPF₆ with a Li-graphite hybrid anode [32]. (Reprinted with permission, 2014, John Wiley & Sons.) (b) Charge, discharge, and theoretical capacity of AcNH-TEMPO symmetric flow cell [29]. (Reprinted with permission, 2016, Elsevier.) (c) Charge and discharge behavior of Me-TEMPO cycled against Li at various charge densities [30]. (Reprinted with permission, 2015, John Wiley & Sons).

A modified TEMPO compound, 4-acetamido-2,2,6,6-tetramethylpiperidine-1-oxyl (AcNH-TEMPO), was investigated to determine how structural changes could improve solubility while maintaining high electrochemical performance [29]. Although the performance metrics did not appear to be significantly improved, AcNH-TEMPO has an advantage over TEMPO in its simpler and cheaper synthesis (Table 4). The cost and ease of synthesis is an important metric when considering the scale-up of redox flow battery electrolytes. The disadvantage of this modified compound is its lowered capacity retention compared to that in the work carried out by Wang, with a fade of 7.4% after 20 cycles (Figure 7b). Active species decay was ruled out as a performance degradation mechanism.

Table 4. Physical and chemical characteristics of TEMPO derivatives [29,30,32].

Compound	Redox Potential (vs. Li ⁺ /Li)	Diffusion Coefficient ($\times 10^{-6} \text{ cm}^2 \text{s}^{-1}$)	Solubility (M) Neutral	Solubility (M) Radical Salt
TEMPO	3.5	11	5.2	-
AcNH-TEMPO	3.63	0.43	>0.5	>0.5
MeO-TEMPO	3.6	-	2.5	-

Takechi et al. demonstrated another modified TEMPO compound that formed an ionic liquid at a similar redox potential and higher solubility than AcNH-TEMPO³⁰. MeO-TEMPO was able to achieve a high energy density but was not able to reach the same solubility as unmodified TEMPO (Table 4). Its capacity was, similar to that of AcNH-TEMPO, lowered compared to unmodified TEMPO, with 16% capacity loss after 20 cycles (Figure 7c). The capacity loss of these modified compounds was likely due to the instability of the reduced compounds. Therefore, there has not yet been a modified TEMPO for this use that has out-performed TEMPO. However, the changes provided by derivatives demonstrate that with the right synthesis, an even-better-performing catholyte could be developed.

2.4. Dialkoxybenzenes and Derivatives

Dialkoxybenzene catholytes are considered good candidates for RFBs due to their favorable reversibility and high oxidation potentials (Figure 8 and Table 5) [34,81]. 2,5-Di-tert-butyl-1,4-bis(2-methoxyethoxy)benzene (DBBB) was originally developed to provide effective overcharge protection in Li-ion batteries [82–84]. Brushett et al. then took interest in the use of DBBB as a catholyte material in NAORFBs³³. They found that DBBB had promising metrics for a redox flow battery. When cycled at 0.05 M, DBBB showed a coulombic efficiency of approximately 70% (Figure 9a). However, the solubility of DBBB is considered low for nonaqueous redox flow batteries [85].

Table 5. Physical and chemical properties of dialkoxybenzenes derivatives [33–35].

Compound	Redox Potential (vs. Li/Li ⁺)	Diffusion Coefficient ($\times 10^{-6} \text{ cm}^2 \text{s}^{-1}$)	Solubility (M) Neutral
BODMA	4.02	45	0.15
BODEA	4.18	11	0.10
6 (25DDB)	3.92	-	0.6
7 (23DDB)	3.98	-	2
DBBB	3.93	1.46	0.4

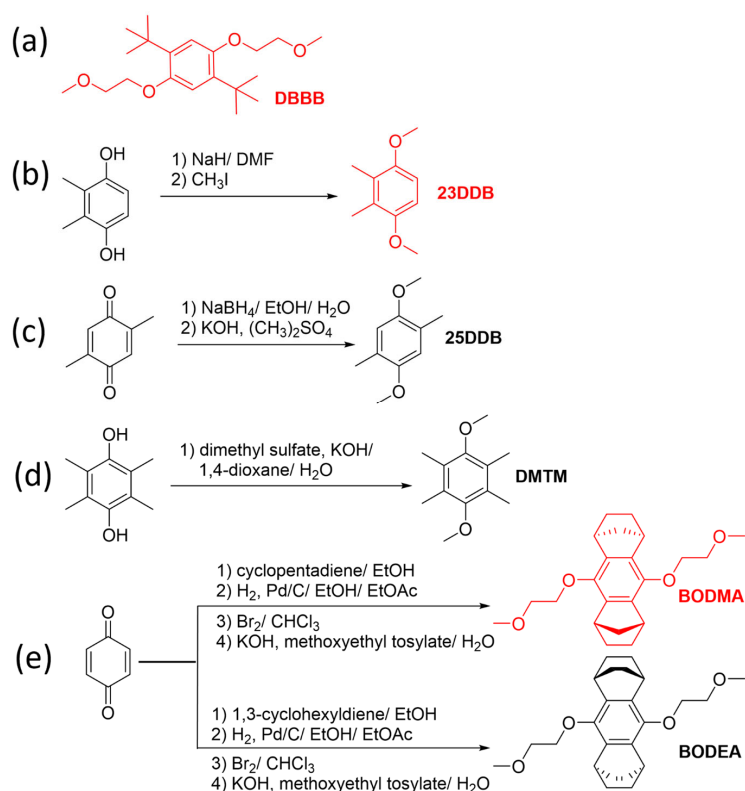


Figure 8. Synthesis of dialkoxybenzenes derivatives. (a) DBBB, (b) 23DDB, (c) 25DDB, (d) DMTM, and (e) BODEA [33–35].

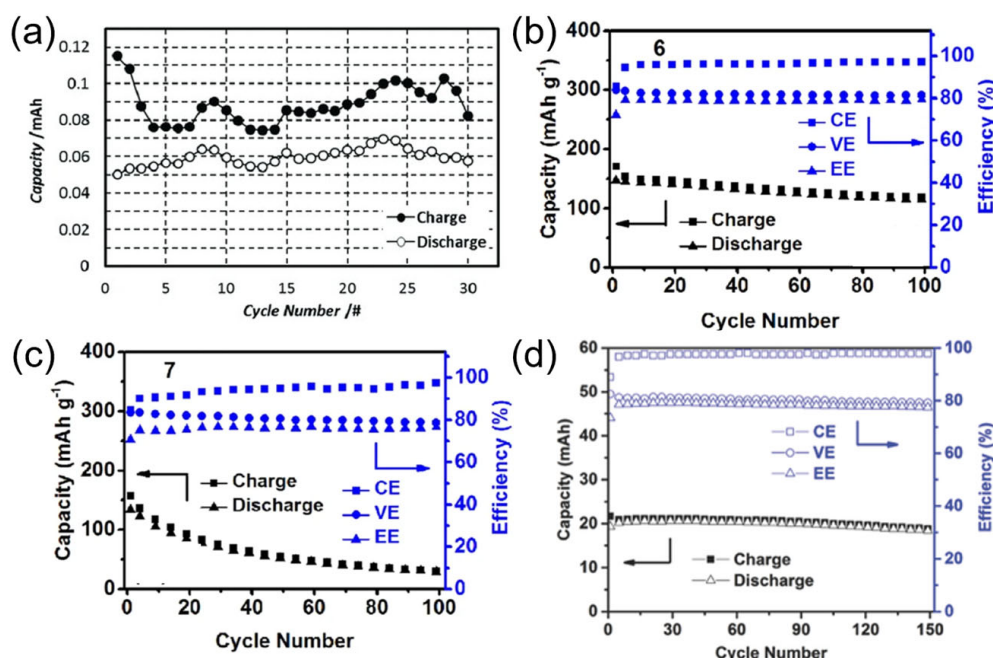


Figure 9. The electrochemical performance of dialkoxybenzene derivatives, with (a) capacity vs. cycle number of 0.05 M DBBB cycled against 0.05 M 2,3,6-trimethylquinoxaline [33]. (Reprinted with permission, 2012, John Wiley & Sons.) (b) Cycling efficiencies and specific capacities over 100 cycles for 25DDB [35]. (Reprinted with permission, 2016, Zhang et al.) (c) Cycling efficiencies and specific capacities for 23DDB [35]. (Reprinted with permission, 2016, Zhang et al.) (d) Capacity and efficiency against cycle number for BODEA cycled against Li at 5 mA cm⁻² [34]. (Reprinted with permission, 2017, John Wiley & Sons).

Zhang's group assessed a variety of dialkoxybenzene derivates while in search for a structure with high capacity that retained good performance otherwise [35]. Among the 11 compounds they examined, 2, referred to as "6" and "7", exhibited promising outcomes. These compounds, "6" and "7", were obtained through the removal of unnecessary steric groups from DBBB, resulting in improved capacity, electrochemical performance, and solubility (Figure 8b,c and Table 5). Compound "6", or 25DDB, displayed minimal capacity fade at 0.2% per cycle (Figures 8b and 9b). On the other hand, compound "7", or 23DDB, exhibited a higher capacity fade of 88% over 100 cycles (Figures 8c and 9c). This divergence was attributed to irreversible side reactions occurring during the cycling of 23DDB.

The compounds 9,10-bis(2-methoxyethoxy)-1,2,3,4,5,6,7,8-octahydro-1,4:5,8-dimethaneno-anthracene (BODMA) and 9,10-bis(2-methoxyethoxy)-1,2,3,4,5,6,7,8-octahydro-1,4:5,8-diethano-anthracene (BODEA) exhibited promising electrochemical performance, while 1,4-dimethoxy-2,3,5,6-tetramethyl-benzene (DMTM) was found to lack electrochemical reversibility [34]. However, the syntheses for these modified dialkoxybenzenes were intricate and lengthy, involving multiple steps and checkpoints to achieve the desired product (as illustrated in Figure 8d,e). Consequently, despite the promising results exhibited by these derivatives, the complexity of their syntheses remains a challenge in the development of modified dialkoxybenzenes. BODMA, chosen for cycling experiments, displayed an exceptional mean capacity retention of 99.97% per cycle over 150 cycles (as shown in Figure 9d). This achievement signifies a notable enhancement in capacity retention when compared to 25DDB and 23DDB.

3. Anodic Redox-Active Organic Molecules

Over the past decade, researchers have been actively working on the development of novel redox-active negolytes with elevated redox potentials, enhanced solubility, and robust electrochemical stability. Pyridinium and viologen are two of the most successful core structures employed in redox-active negolytes. The presence of aromatic rings within these core structures contributes to charge stabilization and structural robustness [86–88]. The incorporation of various functional groups into the negolyte derivatives offers the potential to enhance solubility or adjust redox potentials as needed.

3.1. Pyridinium and Derivatives

As depicted in Figure 10a, the pyridinium core structure comprises a positively charged aromatic ring, featuring a nitrogen atom within the ring to stabilize the positive charge. Sanford's group has played a significant role in developing pyridinium complexes for NAORFB anolytes. They employed a physical organic approach to explore a range of pyridinium derivatives, aiming to fine-tune redox potentials and enhance stability (Figure 10b) [70]. They initiated their exploration with an acyl-pyridinium derivative, designated as "1", which exhibited notable solubility (1.5 M) and displayed a redox potential of -1.08 (the first redox potential) and -1.78 V (the second redox potential) vs. Fc/Fc^+ (Table 6); however, the radical was unstable because of an unknown decay pathway. Through a systematic approach, they identified 17 derivatives, varying in both steric and electronic properties, along the core structure (Figure 10a) [89]. One such derivative, 17, was computationally shown to have a promising radical lifetime, attributed to substituents at the C2 and C6 positions on the pyridine ring. Upon cycling, a 20% capacity fade was observed for 1, and no loss in capacity was evident for 17 (Figure 11a). Their findings revealed that the incorporation of electron-donating substituents in compounds 1–16 led to a negative shift in redox potential, albeit at the expense of stability. Subsequently, by harnessing steric influences with substituents on the nitrogen atom, they successfully decoupled radical stability from redox potential. This innovative strategy holds the potential to streamline the development of advanced catholytes and anolytes for next-generation applications.

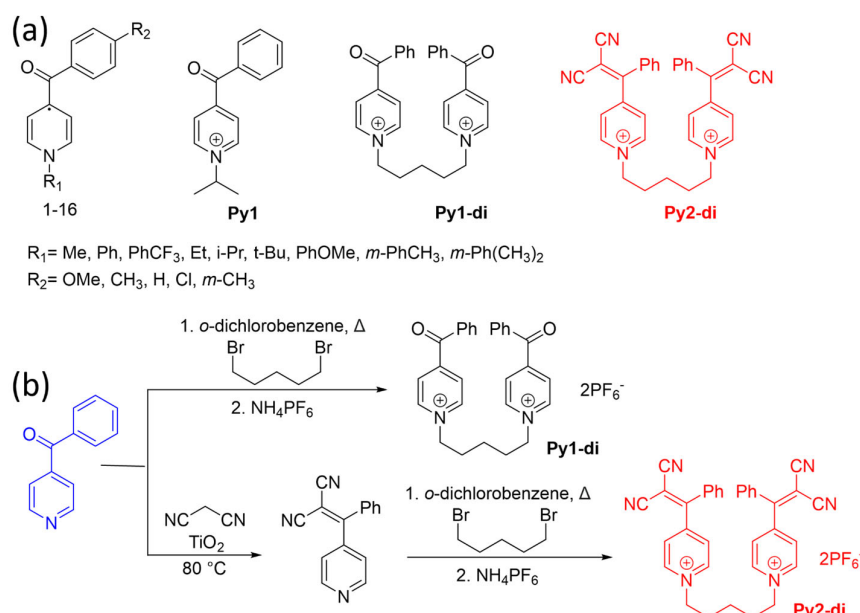


Figure 10. Chemical structures (a) and synthesis (b) of pyridinium derivatives [70,89,90].

Table 6. Physical and chemical properties of pyridinium derivatives [70,89,90].

Compound	1st Redox Potential (vs. Fc/Fc ⁺)	2nd Redox Potential (vs. Fc/Fc ⁺)	Solubility (M)
1	−1.08	−1.78	1.5
17	−1.23	—	—
Py1-di	−1.01	−1.55	—
Py2-di	−0.626	−0.976	1.70

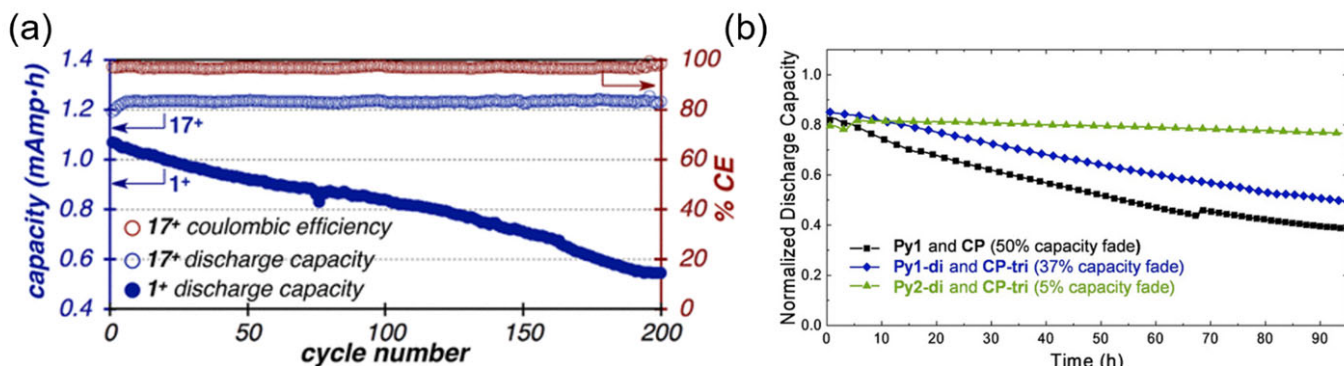


Figure 11. Electrochemical performance of pyridinium derivatives. (a) H-cell cycling of 5 mM of 1 and 17 in symmetric cells [89]. (Reprinted with permission, 2017, American Chemical Society.) (b) Asymmetric flow-cycling data for Py1/CP, Py1-di/CP-tri, and Py2-di/CP0tri [90]. (Reprinted with permission, 2020, John Wiley & Sons).

The crossover rate of redox-active molecules significantly impacts the capacity retention of redox flow cells. To mitigate this crossover rate, the oligocation strategy was employed to synthesize Py1-di from Py1. However, it appears that the carbonyl moiety initially acts as a proton acceptor, rendering the Py1 molecules electrochemically unstable. To address this issue, the reactive carbonyl site was replaced with a less-basic pseudo-oxocarbon malononitrile group. This modification resulted in a substantial increase in the capacity retention of symmetrical cells, as demonstrated in Figure 11b, where Py2-di symmetric cells exhibit a capacity retention of over 95% [90].

3.2. Viologens and Derivatives

Viologen molecules are typically made up of two positively charged nitrogen-containing aromatic rings linked by a bridge. The two pyridiniums bridged together in the viologen facilitate a two-electron redox reaction (Figure 12). Viologens are promising as anolytes due to their inherent two-electron reduction capacity [39]. They have been extensively studied in aqueous flow batteries due to their high solubility and electrochemical stability in aqueous solvents [91–93].

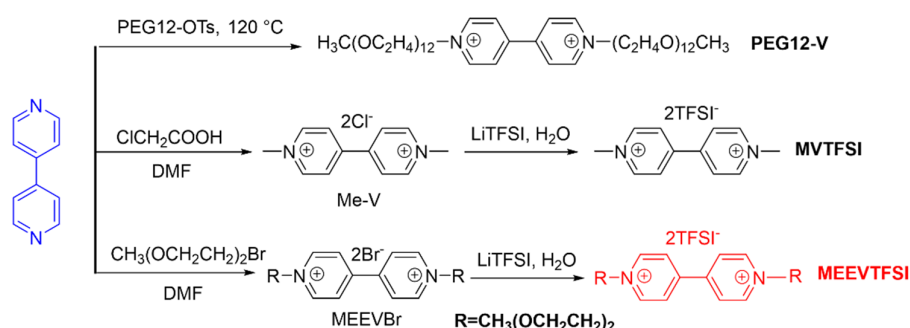


Figure 12. Synthesis of viologen derivatives [23,40,41].

Methyl viologen, in particular, has been frequently used as an anolyte in aqueous redox flow batteries, but only the first reduction of Me-V is accessible in aqueous solutions [40,92,94]. To increase its solubility in non-aqueous solutions, Hu et al. used a bis(trifluoromethane)sulfonamide (TFSI) counter ion and demonstrated that it could be used in a non-aqueous electrolyte to access both redox couples for high energy density and cell voltage (Table 7) [42]. MVTFSI demonstrated 88% capacity retention after 100 cycles (Figure 13a). In an effort to enhance solubility and bolster electrochemical stability in organic solvents, Odom and colleagues modified the parent viologen compound by introducing a 2-(2-methoxyethoxy)ethyl group (Figure 12) to yield MEEVTSI. This alteration resulted in a slight increase in solubility, reaching approximately 1.1 M in MeCN. Notably, the utilization of MEEPT and MEEVTSI₂ as a posolyte and a negolyte in the full cell configuration exhibited remarkable performance, exhibiting negligible MEEVTSI₂ molecular decay even after 100 cycles at a current density of 10 mA cm⁻² (Figure 5b) [36]. Chai et al. adopted a similar approach to modify the molecule, incorporating 12 oxyethylene units (PEG12-V). In comparison to the methylated viologen (Me-V), a PEGylated viologen exhibited a significant enhancement in solubility up to 0.8 M (Table 7) [39]. Meanwhile, the PEGylated viologen demonstrated a slightly higher capacity retention of 99.9% per cycle, whereas the Me-V exhibited a capacity retention of 99.37% per cycle (Figure 13b,c). This observation also suggests an enhanced electrochemical stability attributed to the presence of the PEG12 functional group.

Table 7. Physical and chemical properties of viologen derivatives [36,39,42,95].

Compound	1st Redox Potential (vs. Ag/Ag ⁺)	2nd Redox Potential (vs. Ag/Ag ⁺)	Diffusion Coefficient ($\times 10^{-6}$ cm ² s ⁻¹)	Solubility (M) (MeCN)
PEG12-V	−0.74	−1.15	−	0.79
Me-V	−0.74	−1.15	6	−
MVTFSI	−0.79	−1.20	7.54	0.98
MEEVTSI	−0.79 (vs. Fc ⁺ /Fc)	−1.26 (vs. Fc ⁺ /Fc)	7	1.1
BV	−0.65	−1.1	6.2	0.84

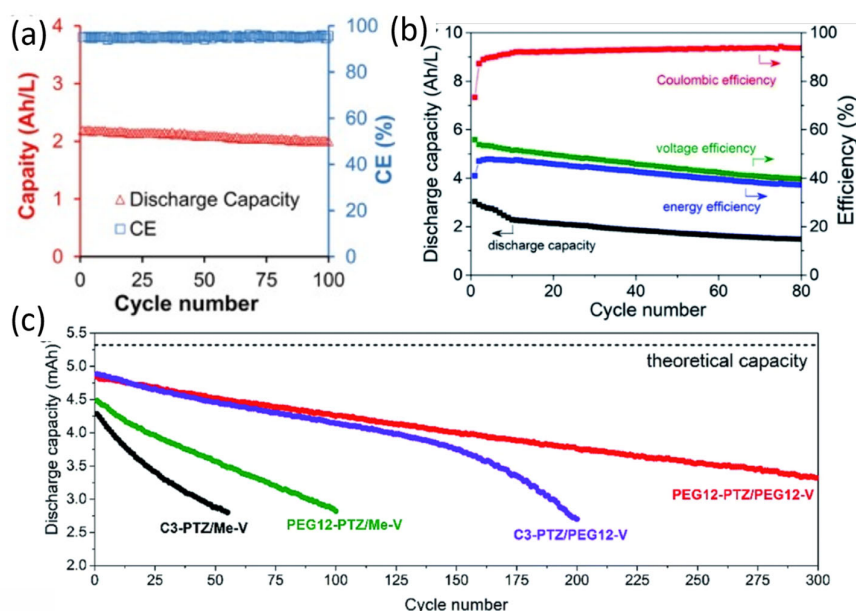


Figure 13. Electrochemical performance of viologen derivatives, with (a) Capacity versus cycle number of FcNTFSI/MVTFSI with a mixed electrolyte (0.1 M FcNTFSI and 0.1 M MVTFSI) for 100 cycles at 30 mA cm^{-2} [42]. (Reprinted with permission, 2018, Elsevier.) (b) Discharge capacity and efficiencies of 240 mM PEG12-PTZ and 100 mM PEG12-V mixed electrolytes [39]. (Reprinted with permission, 2020, Royal Society of Chemistry.) (c) Discharge capacity and efficiencies of PEG12-PTZ/PEG12-V (red), C3-PTZ/PEG12-V (violet), PEG12-PTZ/Me-V (green), and C3-PTZ/Me-V (black) [39]. (Reprinted with permission, 2020, Royal Society of Chemistry).

Mohapatra et al. used a benzylviologen (BV) to produce a high-solubility (0.84 M in acetonitrile) and high-capacity-retention (99% per cycle) non-aqueous redox flow battery [95]. They determined that the degradation of the anolyte did not contribute to any capacity loss. The higher solubility observed was largely attributed to the counter ion, PF_6^- . This solubility increase demonstrates a known fact, that is, counter ions can be just as important as functionalizing the active material for solubility [96–98].

4. Conclusions

This comprehensive review has explored a diverse array of organic catholytes (including the derivatives of quinones, nitroxyl radicals, dialkoxybenzenes, and phenothiazines) and anolytes (comprising viologens and pyridinium derivatives) in the context of non-aqueous organic redox flow batteries. While NAORFBs have emerged as a promising area of energy storage device research, commercialization remains an ambitious goal. The primary challenges are posed by the high costs of materials, driven by complicated synthesis steps and low yields, as well as their low energy density, primarily constrained by the limited solubilities of organic redox molecules and crossover-related issues.

On a positive note, as detailed in this manuscript, several research groups have dedicated significant efforts to designing and synthesizing low-cost organic redox-active molecules with simplified synthesis processes. Notably, one of the catholyte products produced by Dr. Odom's team has already become available for purchase through Tokyo Chemical Industry (TCI). Many other research groups are also actively engaged in the design and synthesis of these innovative molecules.

Through a molecular engineering approach, it has become evident that the strategic introduction or removal of functional groups, with their electron-withdrawing or donating properties, holds the key to precisely tailoring the solubility, stability, and redox potential of these organic materials. In addition to these molecular considerations, the practical aspects of cost and synthesis duration must not be overlooked. The development of universally applicable synthesis protocols can significantly streamline the production

process. Considering these advancements, non-aqueous organic redox flow batteries stand as a highly promising candidate for the realization of large-scale energy storage solutions. Their evolution through molecular engineering continues to drive their potential as a transformative technology in the field of sustainable energy.

Author Contributions: Conceptualization, Z.L.; writing—draft preparation, review, and editing, C.M.D. and Z.L.; data curation, C.E.B., T.Y. and T.L. All authors have read and agreed to the published version of the manuscript.

Funding: This research was not externally funded.

Data Availability Statement: Not applicable.

Acknowledgments: C.B. acknowledges the 2023 NSCI Dean's Fellowship awarded through the Department of Chemistry, University of Colorado Boulder.

Conflicts of Interest: The authors declare no conflict of interest.

References

1. Liang, Z.; Nguyen, T.P.; Attanayake, N.H.; Easley, A.D.; Lutkenhaus, J.L.; Wooley, K.L.; Odom, S.A. Metal-free polypeptide redox flow batteries. *Mater. Adv.* **2022**, *3*, 6558–6565. [[CrossRef](#)]
2. Li, M.; Rhodes, Z.; Cabrera-Pardo, J.R.; Minteer, S.D. Recent advancements in rational design of non-aqueous organic redox flow batteries. *Sustain. Energy Fuels* **2020**, *4*, 4370–4389. [[CrossRef](#)]
3. Huang, Y.; Gu, S.; Yan, Y.; Li, S.F.Y. Nonaqueous redox-flow batteries: Features, challenges, and prospects. *Curr. Opin. Chem. Eng.* **2015**, *8*, 105–113. [[CrossRef](#)]
4. Kwabi, D.G.; Ji, Y.; Aziz, M.J. Electrolyte Lifetime in Aqueous Organic Redox Flow Batteries: A Critical Review. *Chem. Rev.* **2020**, *120*, 6467–6489. [[CrossRef](#)]
5. Kowalski, J.A.; Su, L.; Milshtein, J.D.; Brushett, F.R. Recent advances in molecular engineering of redox active organic molecules for nonaqueous flow batteries. *Energy Environ. Eng. React. Eng. Catal.* **2016**, *13*, 45–52. [[CrossRef](#)]
6. Cameron, J.M.; Holc, C.; Kibler, A.J.; Peake, C.L.; Walsh, D.A.; Newton, G.N.; Johnson, L.R. Molecular redox species for next-generation batteries. *Chem. Soc. Rev.* **2021**, *50*, 5863–5883. [[CrossRef](#)]
7. Hu, B.; De Bruler, C.; Rhodes, Z.; Liu, T.L. Long-Cycling Aqueous Organic Redox Flow Battery (AORFB) toward Sustainable and Safe Energy Storage. *J. Am. Chem. Soc.* **2017**, *139*, 1207–1214. [[CrossRef](#)]
8. Luo, J.; Hu, B.; Hu, M.; Zhao, Y.; Liu, T.L. Status and Prospects of Organic Redox Flow Batteries toward Sustainable Energy Storage. *ACS Energy Lett.* **2019**, *4*, 2220–2240. [[CrossRef](#)]
9. Liang, Z.; Jha, R.K.; Suduwella, T.M.; Attanayake, N.H.; Wang, Y.; Zhang, W.; Cao, C.; Kaur, A.P.; Landon, J.; Odom, S.A. A prototype of high-performance two-electron non-aqueous organic redox flow battery operated at -40°C . *J. Mater. Chem. A* **2022**, *10*, 24685–24693. [[CrossRef](#)]
10. Huang, Z.; Mu, A.; Wu, L.; Yang, B.; Qian, Y.; Wang, J. Comprehensive Analysis of Critical Issues in All-Vanadium Redox Flow Battery. *ACS Sustain. Chem. Eng.* **2022**, *10*, 7786–7810. [[CrossRef](#)]
11. Huang, Z.; Liu, Y.; Xie, X.; Huang, Q.; Huang, C. Experimental study on efficiency improvement methods of vanadium redox flow battery for large-scale energy storage. *Electrochim. Acta* **2023**, *466*, 143025. [[CrossRef](#)]
12. Chao, D.; Qiao, S.-Z. Toward High-Voltage Aqueous Batteries: Super- or Low-Concentrated Electrolyte? *Joule* **2020**, *4*, 1846–1851. [[CrossRef](#)]
13. ECMWF. C3S. Available online: <https://cds.climate.copernicus.eu/cdsapp#/home> (accessed on 31 August 2023).
14. Gong, K.; Fang, Q.; Gu, S.; Li, S.F.Y.; Yan, Y. Nonaqueous redox-flow batteries: Organic solvents, supporting electrolytes, and redox pairs. *Energy Environ. Sci.* **2015**, *8*, 3515–3530. [[CrossRef](#)]
15. Chen, M.; Zhang, J.; Ji, X.; Fu, J.; Feng, G. Progress on predicting the electrochemical stability window of electrolytes. *Curr. Opin. Electrochem.* **2022**, *34*, 101030. [[CrossRef](#)]
16. Izutsu, K. *Electrochemistry in Nonaqueous Solutions*; John Wiley & Sons: Weinheim, Germany, 2009.
17. Ue, M.; Ida, K.; Mori, S. Electrochemical Properties of Organic Liquid Electrolytes Based on Quaternary Onium Salts for Electrical Double-Layer Capacitors. *J. Electrochem. Soc.* **1994**, *141*, 2989. [[CrossRef](#)]
18. Zhang, C.; Zhang, L.; Ding, Y.; Peng, S.; Guo, X.; Zhao, Y.; He, G.; Yu, G. Progress and prospects of next-generation redox flow batteries. *Energy Storage Mater.* **2018**, *15*, 324–350. [[CrossRef](#)]
19. Perry, M.L.; Weber, A.Z. Advanced Redox-Flow Batteries: A Perspective. *J. Electrochem. Soc.* **2015**, *163*, A5064. [[CrossRef](#)]
20. Gregory, T.D.; Perry, M.L.; Albertus, P. Cost and price projections of synthetic active materials for redox flow batteries. *J. Power Sources* **2021**, *499*, 229965. [[CrossRef](#)]
21. Attanayake, N.H.; Kowalski, J.A.; Greco, K.V.; Casselman, M.D.; Milshtein, J.D.; Chapman, S.J.; Parkin, S.R.; Brushett, F.R.; Odom, S.A. Tailoring Two-Electron-Donating Phenothiazines To Enable High-Concentration Redox Electrolytes for Use in Nonaqueous Redox Flow Batteries. *Chem. Mater.* **2019**, *31*, 4353–4363. [[CrossRef](#)]

22. Perera, A.S.; Suduwella, T.M.; Attanayake, N.H.; Jha, R.K.; Eubanks, W.L.; Shkrob, I.A.; Risko, C.; Kaur, A.P.; Odom, S.A. Large variability and complexity of isothermal solubility for a series of redox-active phenothiazines. *Mater. Adv.* **2022**, *3*, 8705–8715. [[CrossRef](#)]
23. Attanayake, N.H.; Liang, Z.; Wang, Y.; Kaur, A.P.; Parkin, S.R.; Mobley, J.K.; Ewoldt, R.H.; Landon, J.; Odom, S.A. Dual function organic active materials for nonaqueous redox flow batteries. *Mater. Adv.* **2021**, *2*, 1390–1401. [[CrossRef](#)]
24. Ding, Y.; Zhang, C.; Zhang, L.; Zhou, Y.; Yu, G. Molecular engineering of organic electroactive materials for redox flow batteries. *Chem. Soc. Rev.* **2018**, *47*, 69–103. [[CrossRef](#)] [[PubMed](#)]
25. Huskinson, B.; Marshak, M.P.; Suh, C.; Er, S.; Gerhardt, M.R.; Galvin, C.J.; Chen, X.; Aspuru-Guzik, A.; Gordon, R.G.; Aziz, M.J. A metal-free organic–inorganic aqueous flow battery. *Nature* **2014**, *505*, 195–198. [[CrossRef](#)] [[PubMed](#)]
26. Wang, W.; Xu, W.; Cosimescu, L.; Choi, D.; Li, L.; Yang, Z. Anthraquinone with tailored structure for a nonaqueous metal–organic redox flow battery. *Chem. Commun.* **2012**, *48*, 6669–6671. [[CrossRef](#)]
27. Cao, J.; Tao, M.; Chen, H.; Xu, J.; Chen, Z. A highly reversible anthraquinone-based anolyte for alkaline aqueous redox flow batteries. *J. Power Sources* **2018**, *386*, 40–46. [[CrossRef](#)]
28. Wu, M.; Jing, Y.; Wong, A.A.; Fell, E.M.; Jin, S.; Tang, Z.; Gordon, R.G.; Aziz, M.J. Extremely Stable Anthraquinone Negolytes Synthesized from Common Precursors. *Chem.* **2020**, *6*, 1432–1442. [[CrossRef](#)]
29. Milshtein, J.D.; Barton, J.L.; Darling, R.M.; Brushett, F.R. 4-acetamido-2,2,6,6-tetramethylpiperidine-1-oxyl as a model organic redox active compound for nonaqueous flow batteries. *J. Power Sources* **2016**, *327*, 151–159. [[CrossRef](#)]
30. Takechi, K.; Kato, Y.; Hase, Y. A Highly Concentrated Catholyte Based on a Solvate Ionic Liquid for Rechargeable Flow Batteries. *Adv. Mater.* **2015**, *27*, 2501–2506. [[CrossRef](#)] [[PubMed](#)]
31. Li, Z.; Li, S.; Liu, S.; Huang, K.; Fang, D.; Wang, F.; Peng, S. Electrochemical Properties of an All-Organic Redox Flow Battery Using 2,2,6,6-Tetramethyl-1-Piperidinyloxy and N-Methylphthalimide. *Electrochim. Solid-State Lett.* **2011**, *14*, A171. [[CrossRef](#)]
32. Wei, X.; Xu, W.; Vijayakumar, M.; Cosimescu, L.; Liu, T.; Sprenkle, V.; Wang, W. TEMPO-Based Catholyte for High-Energy Density Nonaqueous Redox Flow Batteries. *Adv. Mater.* **2014**, *26*, 7649–7653. [[CrossRef](#)]
33. Brushett, F.R.; Vaughney, J.T.; Jansen, A.N. An All-Organic Non-aqueous Lithium-Ion Redox Flow Battery. *Adv. Energy Mater.* **2012**, *2*, 1390–1396. [[CrossRef](#)]
34. Zhang, J.; Yang, Z.; Shkrob, I.A.; Assary, R.S.; Tung, S.O.; Silcox, B.; Duan, W.; Zhang, J.; Su, C.C.; Hu, B.; et al. Annulated Dialkoxybenzenes as Catholyte Materials for Non-aqueous Redox Flow Batteries: Achieving High Chemical Stability through Bicyclic Substitution. *Adv. Energy Mater.* **2017**, *7*, 1701272. [[CrossRef](#)]
35. Huang, J.; Pan, B.; Duan, W.; Wei, X.; Assary, R.S.; Su, L.; Brushett, F.R.; Cheng, L.; Liao, C.; Ferrandon, M.S.; et al. The lightest organic radical cation for charge storage in redox flow batteries. *Sci. Rep.* **2016**, *6*, 32102. [[CrossRef](#)] [[PubMed](#)]
36. Liang, Z.; Attanayake, N.H.; Greco, K.V.; Neyhouse, B.J.; Barton, J.L.; Kaur, A.P.; Eubanks, W.L.; Brushett, F.R.; Landon, J.; Odom, S.A. Comparison of Separators vs Membranes in Nonaqueous Redox Flow Battery Electrolytes Containing Small Molecule Active Materials. *ACS Appl. Energy Mater.* **2021**, *4*, 5443–5451. [[CrossRef](#)]
37. Kowalski, J.A.; Casselman, M.D.; Kaur, A.P.; Milshtein, J.D.; Elliott, C.F.; Modekrutti, S.; Attanayake, N.H.; Zhang, N.; Parkin, S.R.; Risko, C.; et al. A stable two-electron-donating phenothiazine for application in nonaqueous redox flow batteries. *J. Mater. Chem. A* **2017**, *5*, 24371–24379. [[CrossRef](#)]
38. Milshtein, J.D.; Kaur, A.P.; Casselman, M.D.; Kowalski, J.A.; Modekrutti, S.; Zhang, P.L.; Harsha Attanayake, N.; Elliott, C.F.; Parkin, S.R.; Risko, C.; et al. High current density, long duration cycling of soluble organic active species for non-aqueous redox flow batteries. *Energy Environ. Sci.* **2016**, *9*, 3531–3543. [[CrossRef](#)]
39. Chai, J.; Lashgari, A.; Wang, X.; Williams, C.K.; Jiang, J. “Jimmy” All-PEGylated redox-active metal-free organic molecules in non-aqueous redox flow battery. *J. Mater. Chem. A* **2020**, *8*, 15715–15724. [[CrossRef](#)]
40. Janoschka, T.; Martin, N.; Hager, M.D.; Schubert, U.S. An Aqueous Redox-Flow Battery with High Capacity and Power: The TEMPTMA/MV System. *Angew. Chem. Int. Ed.* **2016**, *55*, 14427–14430. [[CrossRef](#)]
41. Chai, J.; Lashgari, A.; Cao, Z.; Williams, C.K.; Wang, X.; Dong, J.; Jiang, J. “Jimmy” PEGylation-Enabled Extended Cyclability of a Non-aqueous Redox Flow Battery. *ACS Appl. Mater. Interfaces* **2020**, *12*, 15262–15270. [[CrossRef](#)]
42. Hu, B.; Liu, T.L. Two electron utilization of methyl viologen anolyte in nonaqueous organic redox flow battery. *J. Energy Chem.* **2018**, *27*, 1326–1332. [[CrossRef](#)]
43. Ahn, S.; Jang, J.H.; Kang, J.; Na, M.; Seo, J.; Singh, V.; Joo, J.M.; Byon, H.R. Systematic Designs of Dicationic Heteroarylpyridiniums as Negolytes for Nonaqueous Redox Flow Batteries. *ACS Energy Lett.* **2021**, *6*, 3390–3397. [[CrossRef](#)]
44. Li, M.; Odom, S.A.; Pancoast, A.R.; Robertson, L.A.; Vaid, T.P.; Agarwal, G.; Doan, H.A.; Wang, Y.; Suduwella, T.M.; Bheemireddy, S.R.; et al. Experimental Protocols for Studying Organic Non-aqueous Redox Flow Batteries. *ACS Energy Lett.* **2021**, *6*, 3932–3943. [[CrossRef](#)]
45. Yao, Y.; Lei, J.; Shi, Y.; Ai, F.; Lu, Y.-C. Assessment methods and performance metrics for redox flow batteries. *Nat. Energy* **2021**, *6*, 582–588. [[CrossRef](#)]
46. Yuan, J.; Pan, Z.-Z.; Jin, Y.; Qiu, Q.; Zhang, C.; Zhao, Y.; Li, Y. Membranes in non-aqueous redox flow battery: A review. *J. Power Sources* **2021**, *500*, 229983. [[CrossRef](#)]
47. Huang, Q.; Wang, Q. Next-Generation, High-Energy-Density Redox Flow Batteries. *Chem. Plus Chem.* **2015**, *80*, 312–322. [[CrossRef](#)]

48. Zhang, J.; Jiang, G.; Xu, P.; Kashkooli, A.G.; Mousavi, M.; Yu, A.; Chen, Z. An all-aqueous redox flow battery with unprecedented energy density. *Energy Environ. Sci.* **2018**, *11*, 2010–2015. [[CrossRef](#)]
49. Chen, H.; Cong, G.; Lu, Y.-C. Recent progress in organic redox flow batteries: Active materials, electrolytes and membranes. *J. Energy Chem.* **2018**, *27*, 1304–1325. [[CrossRef](#)]
50. Pan, F.; Wang, Q. Redox Species of Redox Flow Batteries: A Review. *Molecules* **2015**, *20*, 20499–20517. [[CrossRef](#)] [[PubMed](#)]
51. Zu, X.; Zhang, L.; Qian, Y.; Zhang, C.; Yu, G. Molecular Engineering of Azobenzene-Based Anolytes Towards High-Capacity Aqueous Redox Flow Batteries. *Angew. Chem.* **2020**, *132*, 22347–22354. [[CrossRef](#)]
52. Huang, S.; Zhang, H.; Salla, M.; Zhuang, J.; Zhi, Y.; Wang, X.; Wang, Q. Molecular engineering of dihydroxyanthraquinone-based electrolytes for high-capacity aqueous organic redox flow batteries. *Nat. Commun.* **2022**, *13*, 4746. [[CrossRef](#)]
53. Gerken, J.B.; Anson, C.W.; Preger, Y.; Symons, P.G.; Genders, J.D.; Qiu, Y.; Li, W.; Root, T.W.; Stahl, S.S. Comparison of Quinone-Based Catholytes for Aqueous Redox Flow Batteries and Demonstration of Long-Term Stability with Tetrasubstituted Quinones. *Adv. Energy Mater.* **2020**, *10*, 2000340. [[CrossRef](#)]
54. Tabor, D.P.; Gómez-Bombarelli, R.; Tong, L.; Gordon, R.G.; Aziz, M.J.; Aspuru-Guzik, A. Mapping the frontiers of quinone stability in aqueous media: Implications for organic aqueous redox flow batteries. *J. Mater. Chem. A* **2019**, *7*, 12833–12841. [[CrossRef](#)]
55. Tong, L.; Jing, Y.; Gordon, R.G.; Aziz, M.J. Symmetric All-Quinone Aqueous Battery. *ACS Appl. Energy Mater.* **2019**, *2*, 4016–4021. [[CrossRef](#)]
56. Zhu, X.; Jing, Y. Natural quinone molecules as effective cathode materials for nonaqueous lithium-ion batteries. *J. Power Sources* **2022**, *531*, 231291. [[CrossRef](#)]
57. Ouyang, Z.; Tranca, D.; Zhao, Y.; Chen, Z.; Fu, X.; Zhu, J.; Zhai, G.; Ke, C.; Kymakis, E.; Zhuang, X. Quinone-Enriched Conjugated Microporous Polymer as an Organic Cathode for Li-Ion Batteries. *ACS Appl. Mater. Interfaces* **2021**, *13*, 9064–9073. [[CrossRef](#)] [[PubMed](#)]
58. Ma, T.; Zhao, Q.; Wang, J.; Pan, Z.; Chen, J. A Sulfur Heterocyclic Quinone Cathode and a Multifunctional Binder for a High-Performance Rechargeable Lithium-Ion Battery. *Angew. Chem. Int. Ed.* **2016**, *55*, 6428–6432. [[CrossRef](#)] [[PubMed](#)]
59. Symons, P. Quinones for redox flow batteries. *Curr. Opin. Electrochem.* **2021**, *29*, 100759. [[CrossRef](#)]
60. Wu, M.; Bahari, M.; Fell, E.M.; Gordon, R.G.; Aziz, M.J. High-performance anthraquinone with potentially low cost for aqueous redox flow batteries. *J. Mater. Chem. A* **2021**, *9*, 26709–26716. [[CrossRef](#)]
61. Zhong, F.; Yang, M.; Ding, M.; Jia, C. Organic Electroactive Molecule-Based Electrolytes for Redox Flow Batteries: Status and Challenges of Molecular Design. *Front. Chem.* **2020**, *8*, 451. [[CrossRef](#)]
62. Ding, Y.; Li, Y.; Yu, G. Exploring Bio-inspired Quinone-Based Organic Redox Flow Batteries: A Combined Experimental and Computational Study. *Chem* **2016**, *1*, 790–801. [[CrossRef](#)]
63. Lei, Z.; Wang, W.; Wang, A.; Yu, Z.; Chen, S.; Yang, Y. A MC/AQ Parasitic Composite as Cathode Material for Lithium Battery. *J. Electrochem. Soc.* **2011**, *158*, A991. [[CrossRef](#)]
64. Pahlevaninezhad, M.; Leung, P.; Velasco, P.Q.; Pahlevani, M.; Walsh, F.C.; Roberts, E.P.L.; Ponce de León, C. A nonaqueous organic redox flow battery using multi-electron quinone molecules. *J. Power Sources* **2021**, *500*, 229942. [[CrossRef](#)]
65. Zheng, Y.; Ramos, Á.P.; Wang, H.; Álvarez, G.; Ridruejo, A.; Peng, J. Non-aqueous organic redox active materials for a bicontinuous microemulsion-based redox flow battery. *Mater. Today Energy* **2023**, *34*, 101286. [[CrossRef](#)]
66. Kaur, A.P.; Ergun, S.; Elliott, C.F.; Odom, S.A. 3,7-Bis(trifluoromethyl)-N-ethylphenothiazine: A redox shuttle with extensive overcharge protection in lithium-ion batteries. *J. Mater. Chem. A* **2014**, *2*, 18190–18193. [[CrossRef](#)]
67. Elliott, C.F.; Fraser, K.E.; Odom, S.A.; Risko, C. Steric Manipulation as a Mechanism for Tuning the Reduction and Oxidation Potentials of Phenothiazines. *J. Phys. Chem. A* **2021**, *125*, 272–278. [[CrossRef](#)] [[PubMed](#)]
68. Preet Kaur, A.; Neyhouse, B.J.; Shkrob, I.A.; Wang, Y.; Harsha Attanayake, N.; Kant Jha, R.; Wu, Q.; Zhang, L.; Ewoldt, R.H.; Brushett, F.R.; et al. Concentration-dependent Cycling of Phenothiazine-based Electrolytes in Nonaqueous Redox Flow Cells. *Chem.-Asian J.* **2023**, *18*, e20220171. [[CrossRef](#)]
69. Yan, Y.; Robinson, S.G.; Vaid, T.P.; Sigman, M.S.; Sanford, M.S. Simultaneously Enhancing the Redox Potential and Stability of Multi-Redox Organic Catholytes by Incorporating Cyclopropenium Substituents. *J. Am. Chem. Soc.* **2021**, *143*, 13450–13459. [[CrossRef](#)]
70. Walser-Kuntz, R.; Yan, Y.; Sigman, M.; Sanford, M.S. A Physical Organic Chemistry Approach to Developing Cyclopropenium-Based Energy Storage Materials for Redox Flow Batteries. *Acc. Chem. Res.* **2023**, *56*, 1239–1250. [[CrossRef](#)] [[PubMed](#)]
71. Yan, Y.; Vaid, T.P.; Sanford, M.S. Bis(diisopropylamino)cyclopropenium-arene Cations as High Oxidation Potential and High Stability Catholytes for Non-aqueous Redox Flow Batteries. *J. Am. Chem. Soc.* **2020**, *142*, 17564–17571. [[CrossRef](#)]
72. Yan, Y.; Sitaula, P.; Odom, S.A.; Vaid, T.P. High Energy Density, Asymmetric, Nonaqueous Redox Flow Batteries without a Supporting Electrolyte. *ACS Appl. Mater. Interfaces* **2022**, *14*, 49633–49640. [[CrossRef](#)]
73. Robinson, S.G.; Yan, Y.; Hendriks, K.H.; Sanford, M.S.; Sigman, M.S. Developing a Predictive Solubility Model for Monomeric and Oligomeric Cyclopropenium-Based Flow Battery Catholytes. *J. Am. Chem. Soc.* **2019**, *141*, 10171–10176. [[CrossRef](#)]
74. Yan, Y.; Vogt, D.B.; Vaid, T.P.; Sigman, M.S.; Sanford, M.S. Development of High Energy Density Diaminocyclopropenium-Phenothiazine Hybrid Catholytes for Non-Aqueous Redox Flow Batteries. *Angew. Chem.* **2021**, *133*, 27245–27251. [[CrossRef](#)]
75. Armstrong, C.G.; Toghill, K.E. Stability of molecular radicals in organic non-aqueous redox flow batteries: A mini review. *Electrochim. Commun.* **2018**, *91*, 19–24. [[CrossRef](#)]

76. Hu, B.; Hu, M.; Luo, J.; Liu, T.L. A Stable, Low Permeable TEMPO Catholyte for Aqueous Total Organic Redox Flow Batteries. *Adv. Energy Mater.* **2022**, *12*, 2102577. [[CrossRef](#)]
77. Zhao, Y.; Zhang, J.; Agarwal, G.; Yu, Z.; Corman, R.E.; Wang, Y.; Robertson, L.A.; Shi, Z.; Doan, H.A.; Ewoldt, R.H.; et al. TEMPO allegro: Liquid catholyte redoxmers for nonaqueous redox flow batteries. *J. Mater. Chem. A* **2021**, *9*, 16769–16775. [[CrossRef](#)]
78. Liu, Y.; Goulet, M.-A.; Tong, L.; Liu, Y.; Ji, Y.; Wu, L.; Gordon, R.G.; Aziz, M.J.; Yang, Z.; Xu, T. A Long-Lifetime All-Organic Aqueous Flow Battery Utilizing TMAP-TEMPO Radical. *Chem* **2019**, *5*, 1861–1870. [[CrossRef](#)]
79. Wilcox, D.A.; Agarkar, V.; Mukherjee, S.; Boudouris, B.W. Stable Radical Materials for Energy Applications. *Annu. Rev. Chem. Biomol. Eng.* **2018**, *9*, 83–103. [[CrossRef](#)]
80. Prakash, N.; Rajeev, R.; John, A.; Vijayan, A.; George, L.; Varghese, A. 2,2,6,6-Tetramethylpiperidinyloxy (TEMPO) Radical Mediated Electro-Oxidation Reactions: A Review. *Chem. Sel.* **2021**, *6*, 7691–7710. [[CrossRef](#)]
81. Wei, X.; Pan, W.; Duan, W.; Hollas, A.; Yang, Z.; Li, B.; Nie, Z.; Liu, J.; Reed, D.; Wang, W.; et al. Materials and Systems for Organic Redox Flow Batteries: Status and Challenges. *ACS Energy Lett.* **2017**, *2*, 2187–2204. [[CrossRef](#)]
82. Zhang, L.; Zhang, Z.; Redfern, P.C.; Curtiss, L.A.; Amine, K. Molecular engineering towards safer lithium-ion batteries: A highly stable and compatible redox shuttle for overcharge protection. *Energy Environ. Sci.* **2012**, *5*, 8204–8207. [[CrossRef](#)]
83. Leonet, O.; Colmenares, L.C.; Kvasha, A.; Oyarbide, M.; Mainar, A.R.; Glossmann, T.; Blázquez, J.A.; Zhang, Z. Improving the Safety of Lithium-Ion Battery via a Redox Shuttle Additive 2,5-Di-tert-butyl-1,4-bis(2-methoxyethoxy)benzene (DBBB). *ACS Appl. Mater. Interfaces* **2018**, *10*, 9216–9219. [[CrossRef](#)] [[PubMed](#)]
84. Zhang, J.; Shkrob, I.A.; Assary, R.S.; Clark, R.J.; Wilson, R.E.; Jiang, S.; Meisner, Q.J.; Zhu, L.; Hu, B.; Zhang, L. An extremely durable redox shuttle additive for overcharge protection of lithium-ion batteries. *Mater. Today Energy* **2019**, *13*, 308–311. [[CrossRef](#)]
85. Huang, J.; Cheng, L.; Assary, R.S.; Wang, P.; Xue, Z.; Burrell, A.K.; Curtiss, L.A.; Zhang, L. Liquid Catholyte Molecules for Nonaqueous Redox Flow Batteries. *Adv. Energy Mater.* **2015**, *5*, 1401782. [[CrossRef](#)]
86. Lv, X.-L.; Sullivan, P.; Fu, H.-C.; Hu, X.; Liu, H.; Jin, S.; Li, W.; Feng, D. Dextrosil-Viologen: A Robust and Sustainable Anolyte for Aqueous Organic Redox Flow Batteries. *ACS Energy Lett.* **2022**, *7*, 2428–2434. [[CrossRef](#)]
87. Jin, S.; Fell, E.M.; Vina-Lopez, L.; Jing, Y.; Michalak, P.W.; Gordon, R.G.; Aziz, M.J. Near Neutral pH Redox Flow Battery with Low Permeability and Long-Lifetime Phosphonated Viologen Active Species. *Adv. Energy Mater.* **2020**, *10*, 2000100. [[CrossRef](#)]
88. Hu, M.; Wu, W.; Luo, J.; Liu, T.L. Desymmetrization of Viologen Anolytes Empowering Energy Dense, Ultra Stable Flow Batteries toward Long-Duration Energy Storage. *Adv. Energy Mater.* **2022**, *12*, 2202085. [[CrossRef](#)]
89. Sevov, C.S.; Hickey, D.P.; Cook, M.E.; Robinson, S.G.; Barnett, S.; Minteer, S.D.; Sigman, M.S.; Sanford, M.S. Physical Organic Approach to Persistent, Cyclable, Low-Potential Electrolytes for Flow Battery Applications. *J. Am. Chem. Soc.* **2017**, *139*, 2924–2927. [[CrossRef](#)]
90. Shrestha, A.; Hendriks, K.H.; Sigman, M.S.; Minteer, S.D.; Sanford, M.S. Realization of an Asymmetric Non-Aqueous Redox Flow Battery through Molecular Design to Minimize Active Species Crossover and Decomposition. *Chem.-Eur. J.* **2020**, *26*, 5369–5373. [[CrossRef](#)]
91. Hu, B.; Tang, Y.; Luo, J.; Grove, G.; Guo, Y.; Liu, L.T. Improved radical stability of viologen anolytes in aqueous organic redox flow batteries. *Chem. Commun.* **2018**, *54*, 6871–6874. [[CrossRef](#)]
92. Liu, T.; Wei, X.; Nie, Z.; Sprenkle, V.; Wang, W. A Total Organic Aqueous Redox Flow Battery Employing a Low Cost and Sustainable Methyl Viologen Anolyte and 4-HO-TEMPO Catholyte. *Adv. Energy Mater.* **2016**, *6*, 1501449. [[CrossRef](#)]
93. Liu, Y.; Li, Y.; Zuo, P.; Chen, Q.; Tang, G.; Sun, P.; Yang, Z.; Xu, T. Screening Viologen Derivatives for Neutral Aqueous Organic Redox Flow Batteries. *Chem. Sus. Chem.* **2020**, *13*, 2245–2249. [[CrossRef](#)] [[PubMed](#)]
94. Jang, S.-S.; Park, S.-K.; Yeon, S.-H.; Shin, K.-H.; Song, H.; Kim, H.-S.; Jung, Y.-S.; Jin, C.-S. Methyl Viologen Anolyte Introducing Nitrate as Counter-Anion for an Aqueous Redox Flow Battery. *J. Electrochem. Soc.* **2021**, *168*, 100532. [[CrossRef](#)]
95. Mohapatra, S.K.; Ramanujam, K.; Sankararaman, S. Benzylviologen/N-hexyl phenothiazine based non-aqueous organic redox flow battery in inert condition. *J. Energy Storage* **2023**, *72*, 108739. [[CrossRef](#)]
96. Garcia, S.N.; Yang, X.; Bereczki, L.; Kónya, D. Aqueous Solubility of Organic Compounds for Flow Battery Applications: Symmetry and Counter Ion Design to Avoid Low-Solubility Polymorphs. *Molecules* **2021**, *26*, 1203. [[CrossRef](#)] [[PubMed](#)]
97. Ruan, W.; Mao, J.; Chen, Q. Redox flow batteries toward more soluble anthraquinone derivatives. *Curr. Opin. Electrochem.* **2021**, *29*, 100748. [[CrossRef](#)]
98. Roznyatovskaya, N.; Noack, J.; Mild, H.; Fühl, M.; Fischer, P.; Pinkwart, K.; Tübke, J.; Skyllas-Kazacos, M. Vanadium Electrolyte for All-Vanadium Redox-Flow Batteries: The Effect of the Counter Ion. *Batteries* **2019**, *5*, 13. [[CrossRef](#)]

Disclaimer/Publisher’s Note: The statements, opinions and data contained in all publications are solely those of the individual author(s) and contributor(s) and not of MDPI and/or the editor(s). MDPI and/or the editor(s) disclaim responsibility for any injury to people or property resulting from any ideas, methods, instructions or products referred to in the content.